れ以上になっていた。この結果をもとに、より多くの雑音が混入する場合も想定して、図 4(b)のように復元ゲインテーブルの値は3倍に制限した。

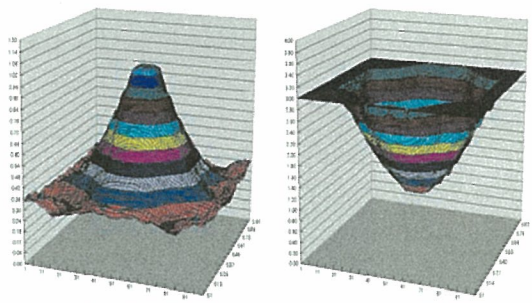

(a)ぼけの周波数特性（二次元）　(b)復元の周波数特性（二次元）

図 4 ぼけの周波数特性と復元の周波数特性

C.研究結果

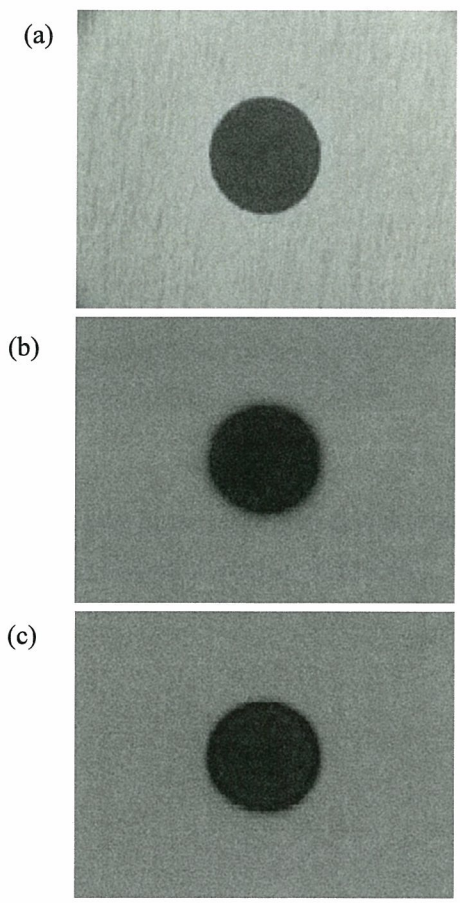

図 5 リファレンス穴の(a)光学顕微鏡像、(b)超音波顕微鏡元画像、(c)超音波顕微鏡画質改善画像

今回測定したボケ関数を利用して、リファレンスに使用した穴の超音波観察画像を復元した結果を図5に示す。

次に同じ100 μmの穴の周囲に約φ130 μmの線のある試料の復元画像を図6に示す。100MHzで18 μmの分解能の穴と周辺の線が分解されて観察することが可能であった。

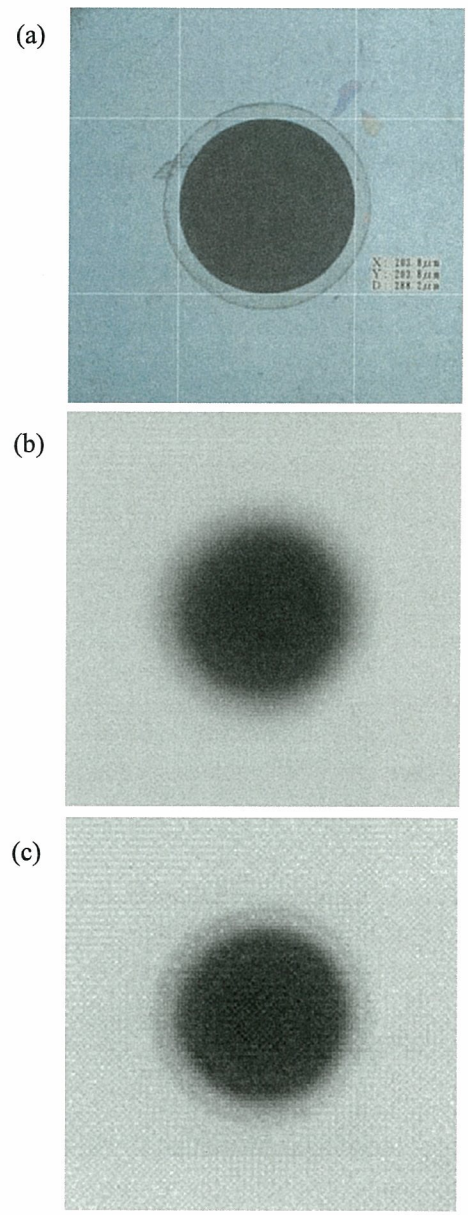

図 6 リング付き穴の(a)光学顕微鏡像、(b)超音波顕微鏡元画像、(c)超音波顕微鏡画質改善画像

実際の生体組織の観察例を処理しても、

図 7（食道）図 8（乳腺）図 9（胃）に示すようにぼけを解消し光学画像に近い画質を得ることができ、臨床の立場でも光学画像のイメージに近くなり、判断がしやすくなったと評価を得た。

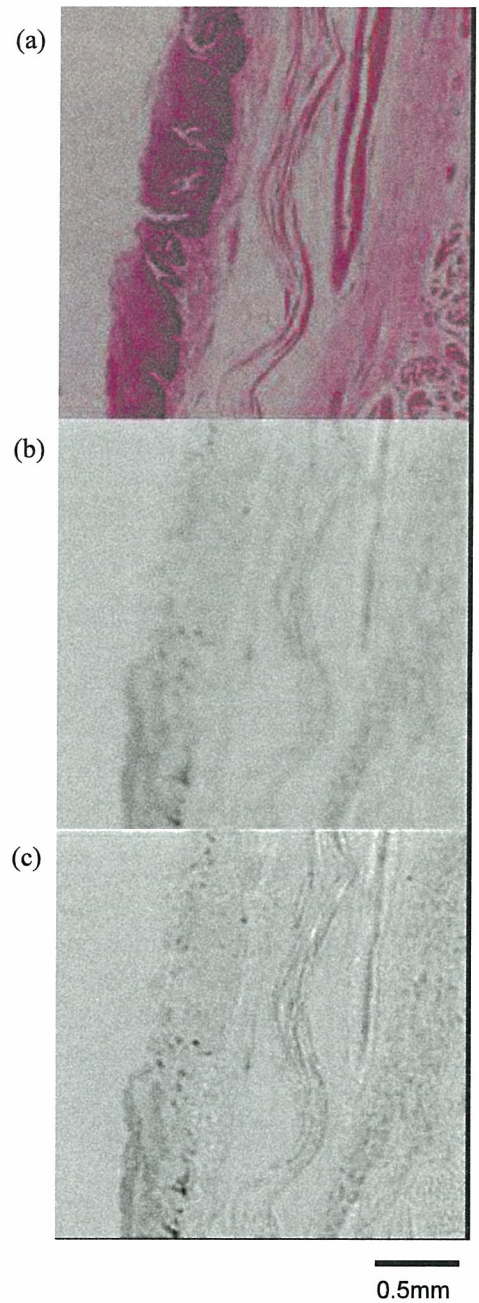

図 7 食道組織の(a)光学顕微鏡像、(b)超音波顕微鏡元画像、(c)超音波顕微鏡画質改善画像

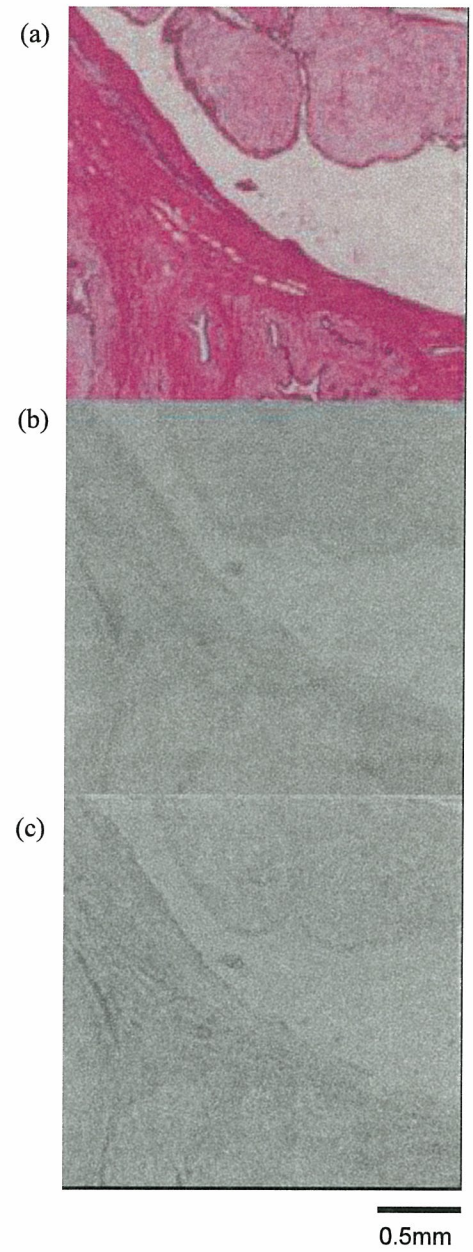

図 8 乳腺組織の(a)光学顕微鏡像、(b)超音波顕微鏡元画像、(c)超音波顕微鏡画質改善画像

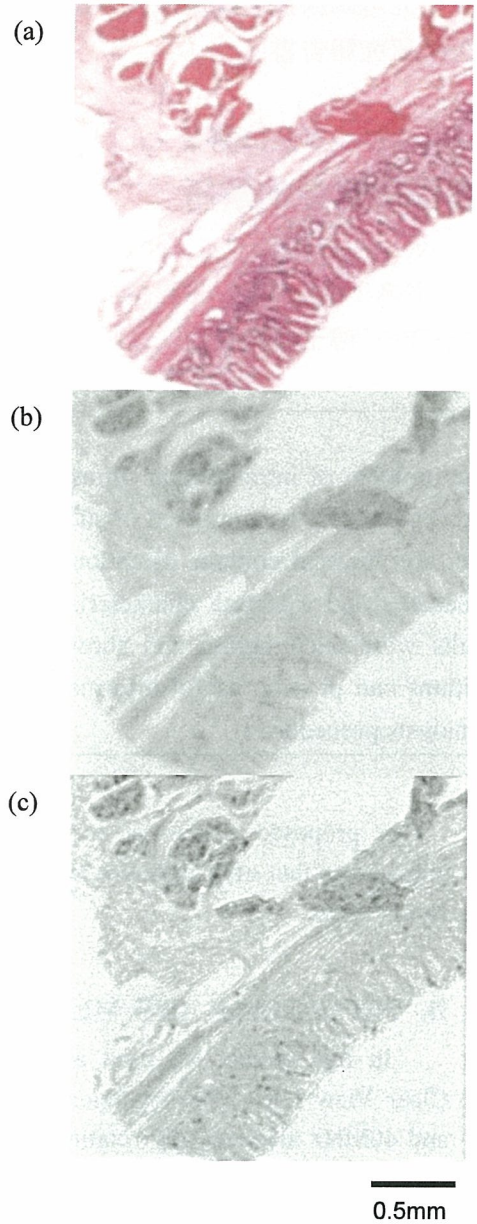

図 9 胃組織の(a)光学顕微鏡像、(b)超音波顕微鏡元画像、(c)超音波顕微鏡画質改善画像

D.結　論

振動子の指向特性を考慮した画像の引き締めを 2DFFT の手法で行なうことで簡単な演算処理で行なうことができるようになった。リファレンスの画像を取得するときの S/N を考慮し、補正値の決定時にノイズ分を含まないようにすることで、実観察において副作用なしに高分解能な観察ができることがわかった。今後、高周波振動子にも適用して細胞の観察などの高分解能が必要な分野での応用を行なっていく。

E.健康危険情報

なし

F.研究発表

F-1.論文

1) Kobayashi K, Hozumi N, Ohtsuki S. Image processing for scanning-type biological ultrasonic microscope considering its beam characteristics. *Proc 9th Sendai Symposium on Ultrasonic Tissue Characterization*. Vol. 1: 36-38, 2006.

F-2.学会発表

F-2-1.国際会議

1) Kobayashi K, Hozumi N, Ohtsuki S. Image processing for scanning-type biological ultrasonic microscope considering its beam characteristics. 4th Joint Meeting of Acoustical Society of America and Acoustical Society of Japan. 2006 年 11 月 30 日.

2)

F-2-2.口頭発表

該当なし

F-3.新聞報道

該当なし

G.知的所有権の取得状況

該当なし

厚生労働省科学研究補助金（萌芽的先端医療技術推進研究事業）
平成１８年度分担研究報告書

生体内超音波ナノ・イメージング法の開発

高周波数超音波画像の定量的解析

分担研究者　エズメラルド　ドス　サントス　フィロ
（東北大学 加齢医学研究所 博士研究員）

ABSTRACT:

A nano-image analysis system applied for the problem of intravascular ultrasound image segmentation and characterization is proposed. The system is comprised of subsystems for calcification detection, tissue characterization, and luminal contour detection. Clustering techniques based on the image texture features and spectral characteristics of the radiofrequency signals were used. The results were encouraging and showed that the proposed image and signal processing algorithms can provide useful information for the medical doctors and automate some of their analysis procedures.

A. OBJECTIVE

It is estimated that cardiovascular diseases cause one-third of total global deaths. Coronary artery disease is a chronic disease in which the coronary arteries gradually harden and narrow in a process called atherosclerosis. As the heart muscle is fed with oxygen-rich blood delivered by the coronary arteries, a blockage in these arteries can cause a heart attack [1].

Currently, several imaging modalities are available to support the diagnosis of coronary artery diseases. X-ray coronary angiography and intravascular ultrasound (IVUS) are examples of the most commonly used diagnostic tools. IVUS has several important advantages over angiography and provide new diagnostic and therapeutic insights for coronary disease. The tomographic orientation of ultrasound enables visualization of the entire circumference of the vessel wall and provides information about tissues beneath the luminal border [2].

The objective of this research is to develop a computer-based system to support medical diagnosis of coronary artery disease.

Our proposed system is comprised of three subsystems that offer different useful information for the user.

B. MATERIALS AND METHODS

In this project we used an IVUS console Clear View Ultra (Boston Scientific Inc., USA) and 40MHz mechanically rotating IVUS catheter Atlantis SR Plus (Boston Scientific Inc., USA). Radiofrequency (RF) data were digitized and stored in a PC (Dell Precision Workstation 330, Dell Inc., USA) using an A/D board GAGE compuscope 8500 (500Msamples/sec., with 8 bits of resolution, Gage Applied Inc., Montreal, Canada) for off-line analysis. The images used were of Windows Bitmap type and the algorithms were developed in Matlab (The Mathworks, Inc., USA).

RF signal data were acquired *in vivo* from 14 human left anterior descending (LDA) coronary arteries at percutaneous transluminal angioplasty. This process was performed in accordance with the ethical principles for medical research involving human subjects. We obtained written

informed consent from all subjects.

1. Subsystem for Calcification Detection

The presence or absence of calcium demonstrated by IVUS has been shown to be an important determinant of the transcatheter interventional success. Calcium is also a known limitation of successful directional atherectomy. Whereas extensive calcium is considered contraindicated, atherectomy is feasible with small, focal areas of calcium [3].

The objective of this subsystem is to detect calcification and calculate the angle of calcification in order to automate this task that is usually done manually by the medical doctors.

As the calcification regions are usually very bright regions in IVUS images they can be segmented by thresholding. However, often, other bright regions of normal tissue may be very bright and can be wrongly segmented as calcification.

This subsystem is based on adaptive thresholding, and an innovative procedure to eliminate wrongly segmented bright regions based on the detection of acoustic shadow.

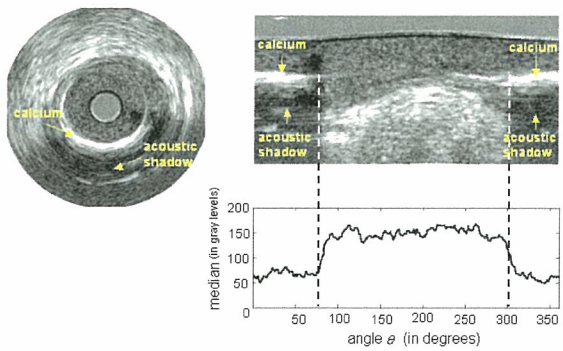

Fig.1 – Example of calcification region and a graph of the median of the polar image columns gray level.

The Fig.1 presents an example of an IVUS image with calcification followed by an acoustic shadow. In the graph below we have the values of the median of the gray level of pixels of each column. We can observe that in the region of shadow there is a drop in the value of median. This is the information used to distinguish which bright regions are really regions of calcification in a given IVUS image.

Using the algorithms for adaptive thresholding and acoustic shadow detection tests were done and some results are shown in the Fig.2. We can observe that in these images the regions of calcification were accurately segmented. The threshold level used for median value was determined empirically.

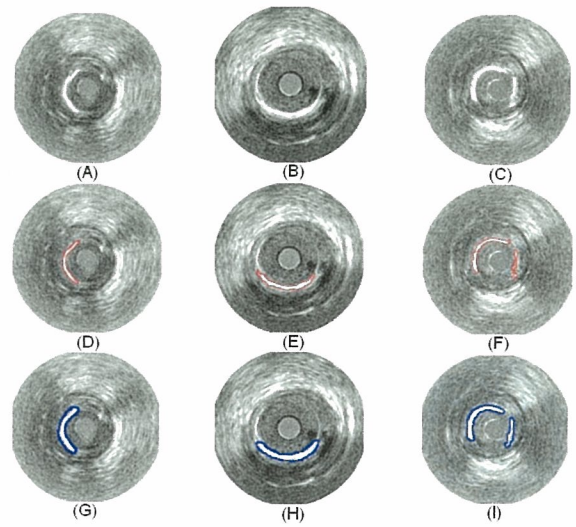

Fig.2 – Results of the calcium detection algorithm. (A), (B), and (C) are the original images. (D), (E), and (F) are the corresponding automatically segmented images. (G), (H), and (I) are the corresponding manually segmented images.

Quantification of Calcium Regions

Methods to quantify calcium in IVUS images typically measure the arc of calcium in a single plane at the target lesion. In order to help the medical doctors in the quantification of the calcified regions in a given IVUS image, we propose here a method for calculus of the angle determined by the arc of calcium.

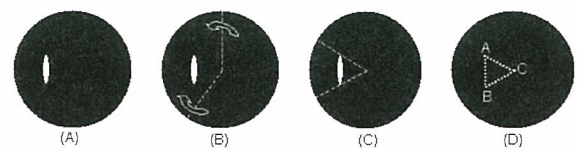

Fig.3 – Example of quantification of calcium region

In order to calculate the angle of the arc of calcium of the segmented calcification, we used

the binary images of the calcium region (Fig.3.A) obtained during the execution of the thresholding algorithm. This image is scanned by two rotating radii in opposing direction until the extreme points of the calcification be found, as shown in the Fig.3(B) and (C). Then, these two extreme points together with the central pixel of the image determine a triangle (Fig.3.D) whose angles can be calculated through trigonometric relations.

This method is summarized in the following algorithm:

Step 1: Determine the extreme points of the interrogated ROI denoted by the capital letters A and B, as shown in the Fig.3.

Step 2: Determine de center of the image (center of catheter), denoted by the capital letter C, and then calculate the length of the sides of the triangle determined by the points A, B, and C.

Step 3: Using the sine and cosine rules, determine the angle of the arc of calcium of the interrogated ROI.

Result I

The Table 1 summarizes the results of the tests. A Receiver Operating Characteristic (ROC) curve was constructed. It is shown in Fig.4. The area under the curve (AUC) is equal to 0.91. The sensitivity was equal to 0.84 and specificity was equal to 0.72.

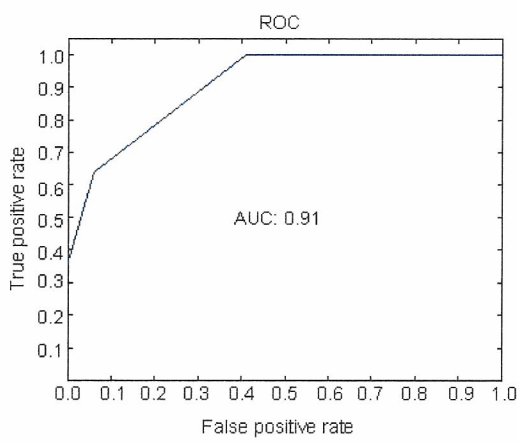

Fig.4 – Receiver operating characteristic curve.

	ROIs correctly classified	ROIs wrongly classified	Total number of ROIs
calcification	21	4	25
normal tissue	13	5	18

Table 1 – Results of calcium detection

Discussion I

The analysis of the images in the polar coordinate system facilitates the process of acoustic shadow detection because is this system the shadow region become confined in a given number of columns forming a rectangular area that can be easily scanned.

Sometimes part of the catheter may be very bright and also, at the same time, present acoustic shadow due to the presence of the guide wire. In cases like this, part of the catheter may be wrongly segmented as calcification. To prevent this problem, a test is done to verify if the centroid of the interrogated ROI is inside the 30 pixels length radius circle centered at the catheter center. This circle corresponds, approximately, to the catheter region. Thus, if a ROI centroid falls inside this circle it would not be considered as a candidate to calcification region. However, the images whose calcification occludes most of the lumen may have the amount of calcification subestimated due to this constraint.

2. Subsystem for Tissue Characterization

The objective of this subsystem is to provide information about the type of tissue presented in an IVUS image. This information is extremely important for medical doctors in order to assess the vulnerability of existing plaques.

FCM Classifier Based on Spectral Parameters

Following the work of Nair *at al.*[4], we assumed that different plaque components would transmit the ultrasound waves at different intensities and could alter the frequency content of the signal by a change in the band width or in the shape of the power spectrum density (PSD). The parameters analyzed were: 1. maximum power; 2.

frequency at maximum power; 3. positive slope; 4. midband fit and 5. y-intercept. These five parameters are represented in the Fig. 5.

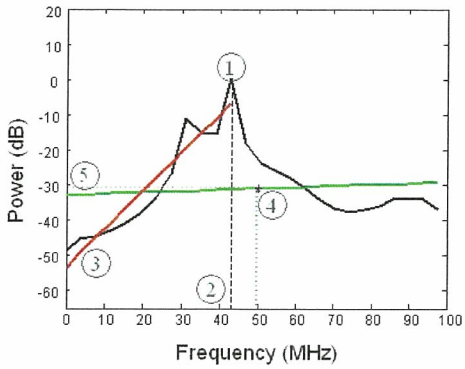

Fig.5 – Example of PSD graph and shape parameters: 1. maximum power, 2. frequency at maximum power, 3. positive slope, 4. midband fit, 5. y-intercept.

The PSD was estimated using Burg method [5].

The problem of image segmentation can regarded as a clustering problem.

The Fuzzy C-means algorithm proposed by Bezdek [6] has long proved to be appropriate for applications in clustering of medical images which, in general, contain considerable amount of blur and noise leading to large degree of uncertainty in the transition between regions.

Thus, in this subsystem we used the Fuzzy C-mean algorithm to characterize the vessel tissues. In order to improve the results, a routine to manually define region of interest was implemented. This routine enable the user to determine two circles. The region between these two circles should contain the vessel walls, and the area outside this region will be ignored (the region in orange color in Fig.6).

Unlike the calcification detection subsystem, this subsystem aims to detect the various types of tissue present in the vessel. However, it does not try to quantify the detected tissues.

Basically, in this system we aim to detect regions of calcification, blood, fibrous tissue, and media. Based in several tests, we realized that five is an appropriate number of clusters.

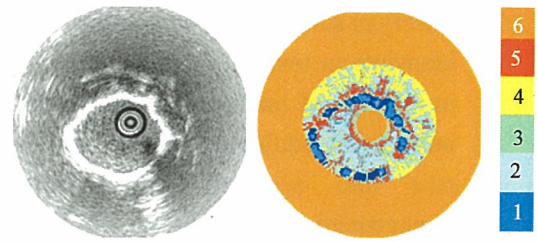

Fig.6 – Echogram and color-code map: 1. calcification, 2. blood, 3. fibrous tissue, 4. acoustic shadow, 5. media, 6. ignored region.

Result II

An example of our preliminary results can be seen in Fig.6. The areas of calcification, lumen, and media were correctly segmented.

As shown in Fig.6, color-codes were used and tissue maps were constructed on IVUS B-mode images by the proposed algorithm.

Discussion II

In preliminary tests done with fuzzy clustering we could observe that the results could be improved by using an optimization scheme. A genetic algorithm, for example, could adapt the number of clusters for each input image. Other membership function parameters also would be optimized to improve the performance of this subsystem that is in its initial phase.

In spite of the encouraging results, the resultant segmentation still need to be validated by histo-logical analysis.

3. Subsystem for Boundary Detection

The objective of this subsystem is to detect the luminal contour in order to assess the degree of vessel occlusion.

Local moments have attracted attention as local features in applications such as edge detection and texture segmentation [7-13]. The main reason for this is that they are inherently integral-based features, so that their use reduce the effect of uncorrelated noise. The computation of local moments, when viewed as a neighborhood operation, can be interpreted as a convolution of the image with a set of masks [13].

Tuceryan successfully proved the efficacy of local moments in texture segmentation [11]. However, in the case of luminal contour detection in IVUS images, an additional feature was necessary to take into account the concentric circular arrangement of artery layers. The feature used to carry this out was the radial distance.

Our texture segmentation algorithm is based on Tuceryan's work [13] and consists of the following steps:

Step 1: Compute the image moments within a small window around each pixel.

Step 2: Compute the texture features from the moments by applying a non-linear transformation followed by an averaging operation.

Step 3: Compute the radial distance.

Step 4: For each pixel in the input image compose a feature vector formed by features computed in step 2 and the radial distance computed in step 3.

Step 5: Perform a fuzzy clustering of the input image pixels on the basis of their feature vectors.

Step 6: Classify every pixel in the input image according to the minimum distance from the center of the clusters found in step 5.

Step 7: Perform a morphological contour smoothing on the segmented image found in step 6.

Step 8: Find the final lumen contour by applying the Sobel operator [14] on the contour smoothed image obtained in step 7.

Our algorithm uses the moments of an image to compute texture features. The $(p+q)$-th order moment m_{pq} of a function of two variables $f(x,y)$ with respect to the origin $(0,0)$ is defined as [13]:

$$m_{pq} = \int_{-\infty}^{\infty}\int_{-\infty}^{\infty} f(x,y)x^p y^q dxdy \qquad (1)$$

where p , q = 0,1,2, … . Normally the moments are computed over some bounded region. If the function is equal to unity within the region and zero outside the region, the lower order moments (small values of p and q) have well defined interpretations. For example, m_{00} is the area of the region, m_{10}/m_{00} and m_{01}/m_{00} give the x and y coordinates of the centroid for the region, respectively. The m_{20}, m_{11} and m_{02} can be used to derive the amount of elongation of the region, and the orientation of its major axis. The higher order moments give even more detailed shape characteristics of the polygons such as symmetry, etc.

In this subsystem, as in Tuceryan's work [13], we regard the intensity image as a function of two variables, $f(x,y)$. We compute a fixed number of the lower order moments for each pixel in the image (we use $p+q \le 2$). The moments are computed within a small local window around each pixel. Given a window size W, the coordinates are normalized to the range of [-0.5 , 0.5] and the pixel is located at the center. The moments are computed with respect to this normalized coordinate system. This permits us to compare the set of moments computed for each pixel. We always choose the window width W to be odd so that the pixel (i , j) is centered on a grid point.

Let (i , j) be the pixel coordinates for which the moments are computed. For a pixel with coordinates (k , l) which falls within the window, the normalized coordinates (x_k, y_l) are given by:

$$x_k = \frac{k-i}{W} \qquad y_l = \frac{l-j}{W} \qquad (2)$$

Then the moment $m_{pq}(i,j)$ within a window centered at pixel (i,j) is computed by a

discrete sum approximation of Equation (1) that uses the normalized coordinates (x_k, y_l):

$$m_{pq}(i,j) = \sum_{k=-W/2}^{W/2} \sum_{l=-W/2}^{W/2} f(i+k, j+l) x_k^p y_l^q \qquad (3)$$

This discrete computation of the set of moments for a given pixel over a finite rectangular window corresponds to a neighborhood operation, and, therefore, it can be interpreted as a convolution of the image with a mask [13].

The motivation for implementing this procedure for detection of the lumen boundary is that the IVUS images usually have very smooth gray-level transition between their regions and also there is noise. These facts make difficult to detect contour of lumen region using only the traditional methods of edge detection like Sobel and Canny operators [14] directly.

Thus in the proposed system we identify the pixels that belong to the lumen region through the clustering based on their texture features and radial position feature. Then we obtain images with regions well defined. After that we can easily detect the lumen contour using the traditional edge detection techniques.

In this work, we define the radial distance R as the distance from the central pixel of the image and the position of the pixel P under consideration. This distance R is normalized and become the seventh feature used in the following clustering of the input image pixels. The radial distance R is of fundamental importance because it helps pixels that are at similar distance from the center of the image to be included in the same cluster if they have similar texture features. The effect of the use of these texture and position features is that the clusters become organized in regions similar to concentric rings around the center pixel. This is associated with physiological structure of the blood vessels as represented in Fig.7.

Clustering

In this block we used the well-known Fuzzy C-Means [6] algorithm. It has been successfully utilized in several image processing applications in the field of medical imaging. This clustering technique uses the feature vectors in order to distinguish the different regions of the image. Through successive iterations of an optimization routine the central vector of each cluster is found. Then the input image pixels are assigned to the cluster whose center vector is the closest to their feature vector.

The number of clusters chosen was four: one cluster for the region between the external wall and adventitia, one for the region between the adventitia and intima, one for the lumen and another one for the catheter zone.

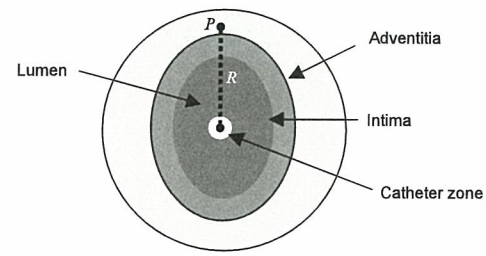

Fig.7 – Illustration of a cross section of a blood vessel. R is the radial distance.

Result III

Using the system presented above, tests were done with 15 IVUS images of different patients. The cases of totally occlusive plaques and large shadow regions were not considered. Some examples of the results are shown in Fig.9 together with the corresponding images that were segmented by a medical doctor for comparison.

We can observe that the boundaries automatically drawn by the proposed system closely resemble the ones drawn manually by a medical doctor. However, some errors can be observed in the dark regions, in general due to shadows that follow hard plaques or due to the guide wire. In these regions, the system tends to segment a region larger than the one that would be segmented by the medical doctor. This occurs

mainly because these darks regions contain no texture information and lead the system to segment based only on the radial distance information. Thus, in the dark regions the system tends to draw lines sometimes far from what the medical doctor would do.

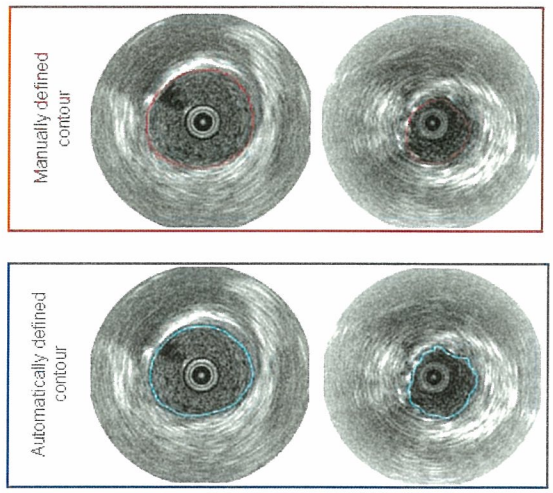

Fig.8- Example of results of the boundary detection algorithm.

In Fig.9 is shown the correlation between areas of the automatically defined lumen and manually defined lumen. The correlation coefficient was equal to 0.87. These images were divided in four quadrants and, for each of them, the areas were calculated individually. With this procedure we could prevent the error compensation.

Discussion III

The transition between the lumen and the vessel wall, as well as the transition between the vessel layers, is quite smooth. This makes boundary detection based on local features a hard task. However, due to the ability of the local moment in distinguishing textured regions together with the radial distance, which is usually small in the lumen region, it was possible to overcome the difficulty caused by the smooth transition between regions. We can also see that the automatically segmented images presented in Fig. 8 closely resemble the images manually segmented.

C. GENERAL DISCUSSION

In order to achieve our ultimate goal of IVUS image segmentation and characterization, we applied a *divide-and-conquer* approach. The task was divided in subtasks carried out by three subsystems.

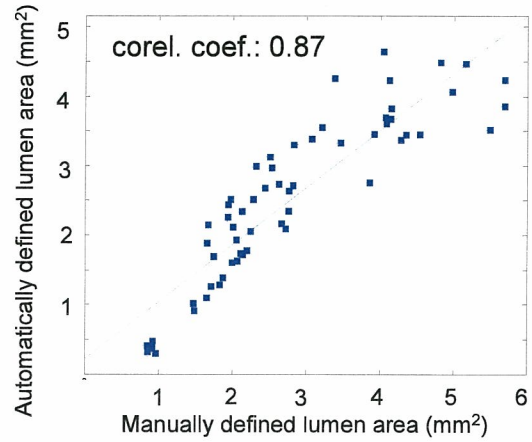

Fig.9 – Graph of the correlation between automatically defined lumen area and manually defined lumen areas.

In spite of some limitations, individually, these subsystems presented encouraging results. However, an integration of these algorithms is still a challenge ahead. This integration is of fundamental importance to make possible the automatic detection of the vulnerable plaques.

It seems that this integration will require an intelligent system capable of represent the expertise of the medical doctors and then extract the useful information from the several output images available and make a final conclusion.

D. CONCLUSION

Visual analysis of medical images by medical doctors is usually accompanied by several limitations associated with interpersonal variations, errors due to fatigue, environmental conditions, etc.

The results obtained in the research have

shown that computer analysis of medical images, if performed with an appropriate logic and with reliable data, can make the medical diagnosis more objective and accurate.

REFERENCES

[1] World Health Organization. Cardiovascular Diseases. Retrieved 11 June 2005, from: http : \ \ www.who.int \ topics \ cardio vascular_diseases \ en \

[2] Kaneda H, Honda Y, Yock PG, Fitzgerald PJ. What do cardiologists want from vascular ultrasound?. In: Saijo Y, van der Steen AFW,ed. Vascular Ultrasound. Tokyo: Springer-Verlag, 2003;3-27.

[3] Scott DS, Arora UK, Farb A, Virmani R, Weissman NJ. Pathologic validation of a new method to quantify coronary calcific deposits in vivo using intravascular ultrasound. Am J Cardiol 85 (2000) 37-40.

[4] Nair A, Kuban BD, Obuchows N, and Vince DG. Assessing spectral algorithms to predict atherosclerotic plaque composition with normalized and raw intravascular ultrasound data. Ultrasound in Medicine and Biology. 10 (2001) 1319-1331

[5] Marple SL, Digital spectral analysis, Prentice Hall, 1987.

[6] Bezdek JC In: Pattern recognition with fuzzy objective function algorithms. New York: Plenum Press. (1981) 65-85.

[7] Chin RT. On image analysis by methods of moments. IEEE Transactions on Pattern Analysis and Machine Intelligence. 10 (1988) 496-513.

[8] Khotanzad A, Hong YH. Invariant image recognition by Zernike moments. IEEE Transaction on Pattern Analysis and Machine Intelligence 12 (1990) 489-97.

[9] Martinez J, Thomas F. Efficient computation of local geometric moments. IEEE Transactions on Image Processing 11 (2002) 1102-11.

[10] Sheynin S, Tuzikov A. Moment computation for objects with spline curve boundary. IEEE Transactions on Pattern Analysis and Machine Intelligence. 25(2003) 1317-22.

[11] Yap P, Paramesran R. Image analysis by Krawtchouk moments. IEEE Transactions on Image Processing 12 (2003) 1367-77.

[12] Suhling M, Arigovindan M, Hunziker P. Multiresolution moment filters: theory and applications. IEEE Transactions on Image Processing 13 (2004) 484-95.

[13] Tuceryan M. Moment based texture segmentation. Proceedings of 11th IAPR International Conference on Image, Speech, Signal Analysis and Pattern Recognition(1992) 45-48.

[14] Gonzales RC and Woods RE In: Digital image processing. New Jersey: Prentice Hall. 2nd ed. (2002) 519-80.

E. INFORMATION ON RISK OF THE HEALTH

None.

F. PRESENTATIONS

1. Papers

[1] Santos Filho E, Yoshizawa M, Tanaka A, Saijo Y, and Iwamoto T. Moment based texture segmentation of intravascular ultrasound images. *Journal of Medical Ultrasoincs*. 32 (2005) 91-9.

[2] Santos Filho E, Yoshizawa M, Iwamoto T, Tanaka A and Saijo Y. Luminal contour detection in intravascular ultrasound images. *Proceedings of the Annual Conference of the Society of Instrument and Control Engineers (SICE 2005)*, pp.1076-1079, Okaiyama, Japan, 2005.

[3] Santos Filho E, Yoshizawa M, Iwamoto T, Tanaka A and Saijo Y. Detection of luminal contour using fuzzy clustering and mathematical morphology in intravascular ultrasound images. *Proc. of The 27th Annual International Conference of the IEEE Engineering in Medicine and Biology Society (EMBS). (on CD-ROM)* Shanghai

– China, 2005.
[4] Saijo Y, Tanaka A, Iwamoto T, Santos Filho E, Yoshizawa M, Hirosaka A, Kijima M, Akino Y, Hanadate Y, and Yambe T. Intravascular two-dimensional tissue strain imaging. *Ultrasonics*. 44 (2006) e147-51..
[5] Saijo Y, Hozumi N, Lee C, Nagao N, Kobayashi K, Okada K, Tanaka N, Santos Filho E, Sasaki H, Tanaka M, and Yambe T. Ultrasonic speed microscopy for imaging of coronary artery. *Ultrasonics*. 44 (2006) e51-5.
[6] Santos Filho E, Saijo Y, Yambe T, Tanaka, A. and Yoshizawa M. Segmentation of calcification regions in intravascular ultrasound images by adaptive threshold. *Proceedings of 19th IEEE International Symposium on Computer-based Medical Systems*. pp.446-451, Salt Lake City – Utah, USA, 2006.
[7] Santos Filho E, Saijo Y, Yambe T, Tanaka A. and Yoshizawa M. A system for tissue characterization and quantification of calcification regions in intravascular ultrasound. *Proceedings of the 2006 IEEE International Ultrasonics Sysmposium*. pp. 1294-1297, Vancouver - BC Canada, 2006.

2. Articles in News Papers

None

G. PATENTS

None.

研究成果の刊行に関する一覧表

書籍

著者氏名	論文タイトル名	書籍全体の編集者名	書籍名	出版社名	出版地	出版年	ページ
Saijo Y	Ultrasonic measurement of micro-acoustic properties of the biological soft materials.	Tribikram Kundu	*Advanced Ultrasonic Methods for Material Characterization*	ISTE	London	2007	89-113
西條芳文	2章 診断—その原理と限界超音波顕微鏡の原理とプラークの評価.	堀正二	冠動脈疾患プロフェッション7 冠動脈疾患の New Concept	中山書店	東京	2006	72-79
西條芳文	1. IVUSの基礎と特性 超音波について.	本江純子、斎藤顕	IVUS マニュアル	中山書店	東京	2006	2-6
西條芳文	8. 冠動脈イメージングの新技術 超音波顕微鏡とintravascular tissue velocity imaging.	本江純子、斎藤顕	IVUS マニュアル	中山書店	東京	2006	308-314

雑誌

発表者氏名	論文タイトル名	発表誌名	巻名	ページ	出版年
van der Steen AFW, Baldewsing RA, Degertekin FL, Emelianov S, Frijlink ME, Furukawa Y, Goertz D, Karaman M, Khuri-Yakub PT, Kim K, Mastik F, Moriya T, Oralkan O, Saijo Y, Schaar JA, Serruys PW, Sethuraman S, Tanaka A, Vos HJ, Witte R, O'Donnell M	IVUS beyond the horizon.	*Eurointerv*	Vol. 2	132-142	2006

Sano H, Hattori K, Saijo Y, Kokubun S	Does decalcification alter the tissue sound speed of rabbit supraspinatus tendon insertion? In vitro measurement using scanning acoustic microscopy.	*Ultrasonics*	Vol. 44, No. 3	297-301	2006
Saijo Y, Hozumi N, Lee C, Nagao M, Kobayashi K, Oakada N, Tanaka N, Santos Filho ED, Sasaki H, Tanaka M, Yambe T	Ultrasonic speed microscopy for imaging of coronary artery.	*Ultrasonics*	Vol. 44; Suppl. 1	e51-55	2006
Saijo Y, Tanaka A, Iwamoto T, Dos Santos Filho E, Yoshizawa M, Hirosaka A, Kijima M, Akino Y, Hanadate Y, Yambe T	Intravascular two-dimensional tissue strain imaging.	*Ultrasonics*	Vol. 44; Suppl. 1	e147-151	2006
Liu H, Saijo Y, Zhang X, Shiraishi Y, Luo Y, Maruyama M, Higa M, Sekine K, Yambe T	Impact of type A behavior on brachial-ankle pulse wave velocity in Japanese.	*Tohoku J Exp Med*	Vol. 209, No. 1	15-21	2006
Saijo Y, Tanaka A, Santos Filho ED, Iwamoto T, Li S, Yoshizawa M, Yambe T	Multiple parametric IVUS imagings for detection of vulnerable plaque.	*Proc 9th Sendai Symposium on Ultrasonic Tissue Characterization*	Vol. 1	13-17	2006
Hozumi N, Terauchi S, Kimura A, Nagao M, Yoshida S, Kobayashi K, Saijo Y	Development of cerebella tissue of rat characterized by acoustic impedance microscope.	*Proc 9th Sendai Symposium on Ultrasonic Tissue Characterization*	Vol. 1	18-21	2006
Sasaki H, Saijo Y, Kanno T, Tanaka M	Classification of flow-limiting thrombus in acute coronary syndrome by acoustic microscopy.	*Proc 9th Sendai Symposium on Ultrasonic Tissue Characterization*	Vol. 1	29-31	2006
Sano H, Hattori K, Komatsuda T, Saijo Y, Sugita T, Itoi E	Tissue sound speed of anterior cruciate ligament in estrogen-controlled rabbits. - A measurement using the scanning acoustic microscope -	*Proc 9th Sendai Symposium on Ultrasonic Tissue Characterization*	Vol. 1	32-35	2006
Kobayashi K, Hozumi N, Ohtsuki S	Image Processing for Scanning-type Biological Ultrasonic Microscope Considering its Beam Characteristics.	*Proc 9th Sendai Symposium on Ultrasonic Tissue Characterization*	Vol. 1	36-38	2006

Sano H, Saijo Y, Kokubun S	Non-mineralized fibrocartilage shows the lowest elastic modulus in the rabbit supraspinatus tendon insertion: measurement with scanning acoustic microscopy.	*J Shoulder Elbow Surg*	Vol. 15, No. 6	743-749	2006
Hagiwara Y, Saijo Y, Chimoto E, Akita H, Sasano Y, Matsumoto F, Kokubun S	Increased elasticity of capsule after immobilization in a rat knee experimental model assessed by scanning acoustic microscopy.	*Upsala J Med Sci*	Vol. 111, No. 3	303-313	2006
Santos Filho E, Saijo Y, Yambe T, Tanaka A, Yoshizawa M	Segmentation of calcification regions in intravascular ultrasound images by adaptive threshold.	*Proc 19th IEEE International Symposium on Computer-based Medical Systems*		446-451	2006
Santos Filho E, Saijo Y, Yambe T, Tanaka A. and Yoshizawa M	A system for tissue characterization and quantification of calcification regions in intravascular ultrasound.	*Proc 2006 IEEE International Ultrasonics Sysmposium*		1294-1297	2006

研究成果の刊行物・別刷

Chapter 3

Ultrasonic measurement of micro-acoustic properties of the biological soft materials

1. Introduction

Optics has been the main observational mode in the microscopic world for many years. However, its domain is restricted to largely transparent media. Sokolov in the former Soviet Union, first proposed the concept of an "ultrasonic microscope" in order to visualize opaque media in 1949 [SOK 49]. He pointed out that the wavelength of 3-GHz ultrasound in water is the same as the wavelength of green light in air. At that time, however, the technologies to produce 3-GHz ultrasound did not exist.

In 1959, Dunn and Fry at University of Illinois developed an "ultrasonic absorption microscope method" with 12-MHz ultrasound [DUN 59]. During the 1970s, high frequency techniques were developed for the microwave technology for radar and for satellite communications. In 1973, Quate and Lemons at Stanford University developed a "scanning acoustic microscope (SAM)" [LEM 73], now used in the biomedical field because of its high resolution and high quality imaging.

We have been applying SAM technology for medical and biological studies at Tohoku University since 1980 [KUS 85] [OKA 85] for the following purposes. First, SAM can be applied for intra-operative pathological examinations since it does not require special staining techniques. The University of California at Irvine group has determined that the obtainable resolution of 600-MHz SAM is sufficient to render a microscopic diagnosis [BAR 91] [JON 96]. We have shown that SAM can classify the types of cancer in stomach [SAI 91] and kidney [SAS 96] by quantitative measurement of ultrasonic attenuation and sound speed at 200-MHz.

Second, ultrasonic data obtained with the high frequency SAM can be used for assessing reflectability or texture in clinical echographic imaging. Density ρ and sound speed c determine the characteristic acoustic impedance Z of the material as

$$Z = \rho c$$

On the assumption that the interface between two fluid-like media is infinite and plane, the relative reflected sound power, in ***dB***, can be determined by the specific acoustic impedance of each medium as

$$dB = 10 \log_{10} \frac{P_r}{P_i} = 10 \log_{10} \frac{(Z_a - Z_b)^2}{(Z_a + Z_b)^2}$$

(***Pr***: sound power reflected at interface, ***Pi***: incident sound power, ***Za***: acoustic impedance of medium ***a***, ***Zb***: acoustic impedance of medium ***b***)

Although the assumption is overly broad for biological media, we have shown that the calculated reflection data and clinical observations are in substantial agreement for myocardium [SAI 97]. Chandraratna et al. also assessed the echo-bright area in myocardium by using 600-MHz SAM [CHA 97].

Third, in its simplest form, the relation between the sound speed and the elastic bulk modulus of liquid-like media is

$$c = \sqrt{\frac{K}{\rho}}$$

(c: sound speed, K: elastic bulk modulus, ρ: density)

As a biological soft tissue may be considered as a liquid-like material, this equation may be applied to assess its elastic properties. Recent biomechanical studies have suggested that the mechanical properties of tissues may not be sufficiently similar to liquids and should be treated as soft solid materials. However, the acoustical relations of solid materials can also be described by the following equation.

$$c = \sqrt{\frac{E(1-\sigma)}{\rho(1+\sigma)(1-2\sigma)}}$$

(c: sound speed, E: Young's modulus, σ: Poisson's ratio, ρ: density)

This relation shows that the Young's modulus of tissue and the sound speed are closely related.

In this chapter, two kinds of scanning acoustic microscope (SAM) systems were employed to characterize the tissue components in biological specimens. In the chapter the potential for higher resolution imaging was also described by showing the examples on cultured cells.

2. Materials and Methods

2.1 Acoustic microscopy between 100 to 200 MHz

Figure 1 is a block diagram of the SAM system developed at Tohoku University. The acoustic focusing element comprises a ZnO piezoelectric transducer with a sapphire lens. The ultrasonic frequency is variable over the range of 100 to 210 MHz and the beam width at the focal volume ranges from 5 μm (at 210 MHz) to 10 μm (at 100 MHz). The focusing element is mechanically scanned at 60 Hz, in the lateral direction (x) above the specimen, which remains stationary on the specimen holder, while the holder is scanned in the other lateral direction (y) in 8 sec, thus providing two-dimensional scanning. The mechanical scanner is so arranged that the ultrasonic beam be transmitted for every 4 μm interval over a 2 mm width. The number of sampling points is 480 in one scanning line and 480 x 480 points make one frame. Both amplitude and phase images can be obtained in a field of view 2mm x 2mm. Either reflection or transmission mode is selectable in the system. In the present study, the reflection mode was chosen. Distilled water, which was maintained at 37°C, was used for the coupling medium between the transducer and the specimen.

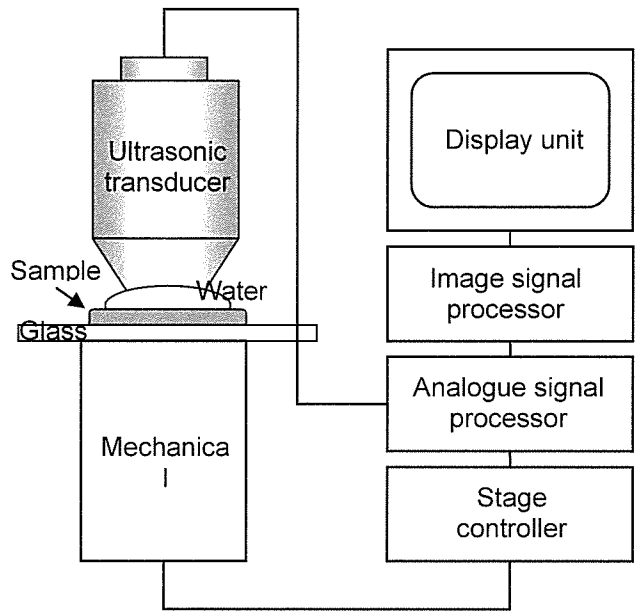

Figure 1. *Block diagram of the scanning acoustic microscope system at Tohoku University.*

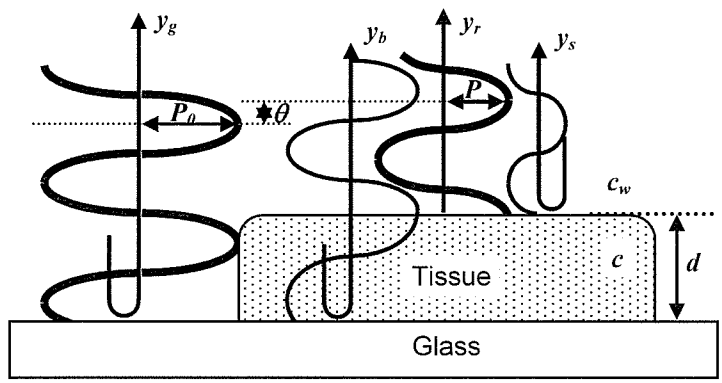

Figure 2. *A schematic illustration of ultrasonic reflections at the tissue.*